Potassium doping of sputtered MoS$_2$ films by CVD method

Ali Altuntepe[1,2,*] , Serkan Erkan[1,3], Mehmet Ali Olgar[1,3], Güldöne Toplu[1], and Recep Zan[1,3,*]

[1] *Nanotechnology Application and Research Center, Niğde Ömer Halisdemir University, Niğde, Turkey*
[2] *Scientific Research Projects Unit, Sivas University of Science and Technology, Sivas, Turkey*
[3] *Department of Physics, Niğde Ömer Halisdemir University, Niğde, Turkey*

ABSTRACT

Doping is an essential approach to enhance the electrical properties of 2D materials. In the present study, two-stage process was used to obtain potassium-doped (K-doped) MoS$_2$. The MoS$_2$ films were grown by magnetron sputtering technique and followed by doping process employing CVD method. The influence of KOH molarity and annealing time on the structural properties of the MoS$_2$ films was investigated thoroughly. 0.2–0.8-M KOH was used to obtain K-doped MoS$_2$. The increase in the molarity of KOH caused a shift in the optical band gap from 1.98 to 1.81 eV. It was observed that increasing the KOH molarity resulted in the loss of homogeneity in the MoS$_2$ films, the use of 0.2-M KOH for the growth of K-doped MoS$_2$ exhibited the most promising results according to performed analyzes. In addition, annealing time also played a critical role in the growth of K-doped MoS$_2$. The dwell times of 5, 10, and 15 min were also used and the effect of molarity and dwell times was investigated. The optical band gap was also shifted from 1.9 to 1.71 eV with increasing the dwell time of KOH. Longer annealing times resulted in the deterioration of the MoS$_2$ film structure. Consequently, an annealing time of 5 min was found to be the optimum value for the growth of K-doped MoS$_2$ film. Overall, this study demonstrates that successful growth of high-quality and homogeneous K-doped MoS$_2$ films which can be employed for various optoelectronic applications.

1 Introduction

The exfoliation process of graphite to form graphene film has been contributed to increase in interest to the two-dimensional (2D) materials. Among these materials, the transition metal chalcogenides (TMDs) are the most studied materials which shows semiconductor behavior and consist of a metal and two chalcogen atoms, represented by the MX$_2$ (M: Mo, Zr, Hf, W and X: S, Se, Te) form, in contrast to the semi-metal structure of graphene [1, 2]. In addition, the TMDs materials exhibit indirect band gap structure in the bulk form [3]. However, when TMDs are isolated from the bulk forming thin film, the indirect band gap structure transforms into the direct band gap form [4]. This direct band transition creates a large photoluminescence effect in the material, contributing to a strong optical absorption, and this paves the way for TMDs

to be preferred for optoelectronic and photovoltaic applications.

The MoS_2 stand out among the TMDs material group due to its superior properties. The monolayer MoS_2 film, which is a 2D material, has an electron mobility of about 200 $cm^2V^{-1}s^{-1}$, an optical transmission of ~ 85%, exhibiting natural n-type behavior, and a band gap of about 1.8 eV [5–8]. The MoS_2 films have the potential to be used as an alternative n-type layer in thin-film third-generation solar cell applications due to their n-type electrical conductivity, high transparency, and suitable optical band gap value. The highest power conversion efficiencies (PCEs) have been achieved in thin-film single-junction transition metal dichalcogenide (TMD) solar cells, specifically 2.8% in plasma-doped MoS_2 and 6.3% in electrostatically doped $MoSe_2$ solar cells [9, 10]. TMDs are commonly transferred onto flexible substrates for flexible solar cell fabrication, but this process can result in damage to the TMD interfaces and the presence of unwanted polymer residues. The challenges are related to a reliable and practical vertical device architecture. In a remarkable achievement, Koosha Nassiri Nazif et al. have achieved a record power conversion efficiency (PCE) of 5.1% for flexible TMD solar cells [11]. This PCE puts TMD solar cells on par with established thin-film solar technologies, such as cadmium telluride, copper indium gallium selenide, amorphous silicon, and III–V. The significance of this achievement is that it opens up new possibilities and applications. TMD solar cells have the potential to reach PCE of up to 5.1%, opening up unprecedented opportunities in industries ranging from aerospace to wearable and implantable electronics. This breakthrough positions TMD solar cells as a promising technology with the ability to revolution power generation in various fields, paving the way for greater efficiency and versatility in energy harvesting applications. Additionally, the MoS_2 in its natural state has 1T, 2H, and 3R phases with trigonal prismatic coordination. Polymorphism is a defining characteristic found in all layered transition metal dichalcogenides, with materials like MoS_2 exemplifying this phenomenon. Depending on how sulfur (S) and molybdenum (Mo) atoms are arranged, triple layers can take on one of three distinct configurations. The trigonal prismatic arrangement gives rise to the semiconducting 2H phase, while an octahedral configuration lead to the metallic 1T phase. In the 1T phase, atoms form a distorted octahedral structure, creating a unique zigzag Mo–Mo chain pattern.

Beyond these variations within the layers, there are additional possibilities for the overall bulk symmetry, including trigonal, hexagonal, and rhombohedral symmetries. These structural variations contribute to the diverse properties and behaviors observed in layered transition metal dichalcogenides [12]. While the 2H phase is the main structure of the film, the 3R phase is often formed during growth process under high temperature and pressure [13]. While 2H/3R-MoS_2 phase shows semiconductor behavior, 1T phase reveals metallic behavior, [14]. The 2H phase is a more dominant and stable phase than the 3R phase, which turns into 2H phase as a result of heating the 3R phase. The 2H and 1T phases coexist in MoS_2 materials in many applications. Although the crystal structures of different phases of materials may have similarity, their electronic structures can be significantly different [15, 16]. Moreover, the 1T phase can be converted to the 2H phase using appropriate annealing conditions.

MoS_2 doping is significant in material science due to its potential to tailor the electronic, optical, and chemical properties of the material. By intentionally introducing impurities or foreign atoms into MoS_2, its conductivity, bandgap, and catalytic activity can be modified to suit for specific applications. One of the significant benefits of MoS_2 doping is the controlled manipulation of its electrical properties, transforming it from an insulator to a semiconductor or even to a metal based on dopant type and concentration. This tunability is essential for designing electronic devices, like transistors and sensors.

Furthermore, specific dopants can strengthen the mechanical properties of MoS_2 or improve its thermal stability, expanding its potential for various applications. By altering its properties through doping, researchers can explore and develop a wide range of applications, such as electronics, sensors, catalysts, and energy storage systems. Doping MoS_2 also offers valuable insights into the fundamental physics and chemistry of two-dimensional materials, contributing to the advancement of nanomaterials as a whole. As research in nanomaterials and 2D materials continues to progress, doping of MoS_2 will be significant in various fields which is likely to grow, opening up new opportunities for technological advancements and innovation.

In the case of 2D-MoS_2 films, doping strategy can be used to modify their electronic band structure, which affects their electrical and optical properties. The doping is a process of intentionally introducing

impurities/foreign atoms into a host material to modify its electrical/optical properties. There are lots of doping methods for 2D materials but these are commonly classify as direct and post-treatment doping [17]. Direct doping is a process in which dopant atoms are introduced into a material during its growth. This approach involves intentionally incorporating dopant atoms into the crystal lattice of material during the growth, resulting in a doped material with specific electronic and optical properties. For the 2D-MoS$_2$ films, direct doping can be achieved by growing the films using dopant-containing precursors or by introducing dopant atoms into the growth environment during the chemical vapor deposition (CVD) [18]. One common approach to direct doping of MoS$_2$ is to use precursor gases containing dopant atoms, such as nitrogen (N), phosphorus (P), or sulfur (S) during the CVD growth [19, 20]. Direct doping can be a powerful tool for tuning the electronic and optical properties of MoS$_2$ films, but it requires fine control of the doping concentration and growth conditions to achieve the desired properties. Additionally, direct doping can also introduce defects and impurities that may adversely affect the performance of material, so careful optimization and characterization of the doping process is necessary [21]. On the other hand, post-treatment doping is a process in which dopant atoms are introduced into a host material after its initial growth. This approach is often used to modify the electronic and optical properties of a material without altering its physical structure or morphology [17]. For 2D-MoS$_2$ films, post-treatment doping can be achieved by introducing dopant atoms through a variety of methods, such as ion implantation, CVD, or solution-based techniques. Post-treatment doping can be used to achieve controlled doping of MoS$_2$ films and modify their electrical and optical properties. However, it is important to note that post-treatment doping can also introduce some defects/impurities that may negatively affect the performance of the materials, so as in the direct doping careful optimization and characterization of the doping process is necessary [22]. Post-treatment method involves introducing dopant atoms into a material after its initial synthesis or growth, allowing for the precise tailoring of its properties. One significant advantage is the flexibility to control dopant concentration independently from the growth conditions, providing a broader range of achievable properties. Post-treatment doping is particularly valuable for retrofitting existing materials, enhancing

their performance without starting the synthesis process from scratch. The non-destructive nature of this method allows for doping completed devices or structures without compromising their integrity. Additionally, post-treatment doping enables selective doping of specific regions, facilitating the creation of complex device structure. The applications of post-treatment doping span across electronics, optoelectronics, catalysis, and energy storage, driving technological advancements in various industries.

Post-treatment doping strategy for 2D-MoS$_2$ films can be done with different ways. For instance, one of the post-treatment strategy involves introducing impurities, such as transition metal atoms, into the MoS$_2$ lattice [23]. This can be done by depositing a layer of the dopant material on top of the MoS$_2$ film and then annealing the sample at high reaction temperature to allow diffusion of the dopant atoms into the MoS$_2$ lattice. The dopant atoms can either donate or accept electrons from the MoS$_2$, resulting in the formation of either n-type or p-type material, respectively [24]. Overall, the choice of doping strategy for 2D-MoS$_2$ films depends on the desired electronic properties and the specific application of the material [25, 26].

Alkali metal doping of MoS$_2$ has been shown as a useful strategy to enhance electronic and optical properties of MoS$_2$ by introducing extra electrons to the conduction band. Alkali metals have a low ionization energy and can easily donate an electron to the MoS$_2$ lattice, resulting in n-type doping [27–29]. With this type of doping, the n-type behavior of MoS$_2$ films can be enhanced by improving the surface charge transfer. It has been demonstrated in theoretical and experimental studies that the alkali metals sodium (Na) and potassium (K) elements are effective n-type additives [30, 31]. The K has smaller electron affinity, so it is a strong electron donor to many material surfaces. The introduction of K ions can have profound effects on the properties of MoS$_2$. K is an alkali metal with a single valence electron and its incorporation can lead to changes in the electronic structure of the material. K atoms bind to the sulfur atoms in MoS$_2$. This binding can occur at the edges of the MoS$_2$ sheets or on their surfaces. The binding of K to sulfur atoms helps to stabilize the MoS$_2$ structure and also improves its catalytic activity in the context of K interaction with MoS$_2$, several key bonding mechanisms come into play. Firstly, there is the formation of K–O bonds, where potassium

atoms bond with the oxygen atoms present in MoS_2. These K–O bonds are characterized by their strength and are instrumental in stabilizing the MoS_2 structure. Another important interaction is K–C bonding, where potassium atoms form bonds with the carbon atoms in MoS_2. Although K–C bonds are generally weaker than K–O bonds, they still contribute to the structural stability of MoS_2 and have implications for enhancing its catalytic activity [32]. Furthermore, the process involves charge transfer. Potassium atoms, being alkali metals with a single valence electron, readily donate this electron to MoS_2. This charge transfer leads to an increase in the number of free electrons within the MoS_2 structure, resulting in improved electrical conductivity. In summary, the interplay between K–O and K–C bonding, along with charge transfer, significantly influences the structural stability and electronic properties of MoS_2, making it a promising avenue for various applications, particularly in the field of materials science and nanotechnology. T. Miyake et al. showed the effect of K doping is not a simple charge transfer. A state arising from the almost free electron state occur at the Fermi level, and aid to conductivity [33]. J. Kong and et al. prepared K-doped semiconducting single-walled carbon nanotube (SWCNT) and they enhanced electrical properties of SWCNT with K doping [34]. Takatoshi Yamada et al. synthesized n-type graphene film layers by wet-transfer process and dipping into the KOH solution [35].

In this study, K-doped MoS_2 thin films were synthesized by two-step method. First step of growth process is deposition of MoS_2 layers by RF magnetron sputtering method employing single sputtering target. Second step of the growth process is K doping of MoS_2 layers by CVD method. Doping is a crucial method to modify MoS_2's electronic and optical properties, allowing for the transformation of its electrical conductivity and band gap. The use of K doping is explored, focusing on its ability to introduce extra electrons to the conduction band, resulting in n-type behavior. The study aims to synthesize K-doped MoS_2 thin films through a two-step process, investigating the molarity ratio of KOH and annealing time for achieving consistent doping with high homogeneity.

2 Material method

2.1 The cleaning process

The RF magnetron sputtering method was used to deposit highly uniform MoS_2 thin films. Before the growth process, the 2.5 × 2.5 cm size of soda–lime glass (SLG) substrates were cleaned in ultrasonic bath using acetone, isopropanol, and distilled water for 5, 5, and 10 min, respectively. Then, cleaned substrates were dried under flow of nitrogen gas.

2.2 The growth process

The cleaned glass substrates were then placed to the sample holder of Physical Vapor Deposition (PVD) system. The samples were positioned 12 cm away to the sputtering target (RF gun) as a parallel in the PVD system. The system shown in Fig. 1a. The MoS_2 films were deposited with the RF source using a single MoS_2 target composed of 95% molybdenum (Mo) and 5% sulfur (S). All growth parameters are given in Table 1. The base and growth pressure of the sputtering chamber were set to around 2×10^{-6} Torr and 1×10^{-3} Torr, respectively. The deposition power density is 40 W and all films were grown with 0.1 Å/s deposition rate. The film thickness used is about 15 nm. In addition, 8-rpm rotation speed and 400 °C substrate temperature was applied during the deposition of the MoS_2 films. These parameters were determined according to the literature and our previous studies [36–38].

2.3 The doping process

Both annealing and doping processes for MoS_2 films were performed in the CVD system (Fig. 1b). Used doping parameters in the CVD system are given in

Table 1 Deposition parameters used in PVD system for growing MoS_2 films

Growth parameters	
Base pressure (Torr)	$<2 \times 10^{-6}$
Growth pressure (Torr)	1×10^{-3}
RF power (Watt)	40
Growth rate (Å/s)	0.1
Rotation (rpm)	8
Substrate temperature (°C)	400
Thickness (nm)	15

Table 2. The 10 ml of KOH source was used as a K source with 0.2, 0.4, 0.6, and 0.8 M in order to prepare K-doped MoS_2 films. Moreover, the doping process was carried out under 10^{-1} Torr pressure for 5-min dwelling time under 50 sccm Argon flow through all processes. Annealing temperature was set to 250 °C according to literature and our previous experiences [39]. The precursor films were heated to 250 °C reaction temperature employing heating rates of 14 °C/min to investigate potential effects of K molar ratio on the properties of the MoS_2 films (see Fig. 1c). After determining the most promising doping molarity as a result of the analyses made, the dwell time was changed from 5 to 15 min with 14 °C/min increments by keeping the heating rate constant. (see Fig. 1c).

Raman spectroscopy and spectroscopic ellipsometer (J.A. Woollam) were used to characterize structural and optical properties of MoS_2 films. The surface microstructure of the films was characterized using the Scanning Electron microscope (SEM) method. X-ray photoelectron spectroscopy (XPS) was used to determine doping ratio and binding energy of MoS_2.

Table 2 Doping parameters of the K-doped MoS_2 films by CVD method

Doping parameters	
Dopant	K
Molarity (M) of 10-ml K source	0.2; 0.4; 0.6; 0.8
Pressure (Torr)	10^{-1}
Dwell time (min.)	5, 10, 15
Carrier gas	Ar
Temperature (°C)	250

3 Results and discussion

The structural properties of pristine MoS_2 films grown by the magnetron sputtering method were initially analyzed by Raman spectroscopy. MoS_2 films have A_{1g} and E_{2g}^1 two main characteristic modes. The A_{1g} mode is related to the out-of-plane vibration of S atoms and the E_{2g}^1 mode is associated with the in-plane vibration of Mo and S atoms [40]. The increasing frequency difference between these two modes, E_{2g}^1–A_{1g}, and shifting the PL emission to longer wavelengths indicate formation of thicker MoS_2 film [41, 42]. In addition, when the E_{2g}^1–A_{1g} frequency difference is approximately 20 cm^{-1} or lower, it indicates formation of a single-layer configuration of MoS_2 [43–46].

The Raman spectra of pristine and varied K-doped MoS_2 films are given in Fig. 2. In the Raman spectra, the E_{2g}^1 and A_{1g} peak positions were observed at around 390 and 410 cm^{-1}, respectively. The decrease or increase in the difference between E_{2g}^1 and A_{1g} modes can be associated with the desorption of various molecules from the MoS_2 surfaces [47]. If the peak intensity of E_{2g}^1 is higher than A_{1g}, which is associated with the single-layer MoS_2 films. The decrease intensity of E_{2g}^1 relative to the effect of film layers can be attributed to less interlayer coupling of the in-plane E_{2g}^1 mode. The intensity ratio of E_{2g}^1 and A_{1g} modes also shows different behaviors for single-layer or multilayer samples. Lee et al. reported that the frequency of the E_{2g}^1 mode decreases with increasing layer thickness [48]. The KOH solutions were used as a K dopant with different molarities (0.2–0.8 M) and the Raman spectra of K-doped MoS_2 are given in Fig. 2.
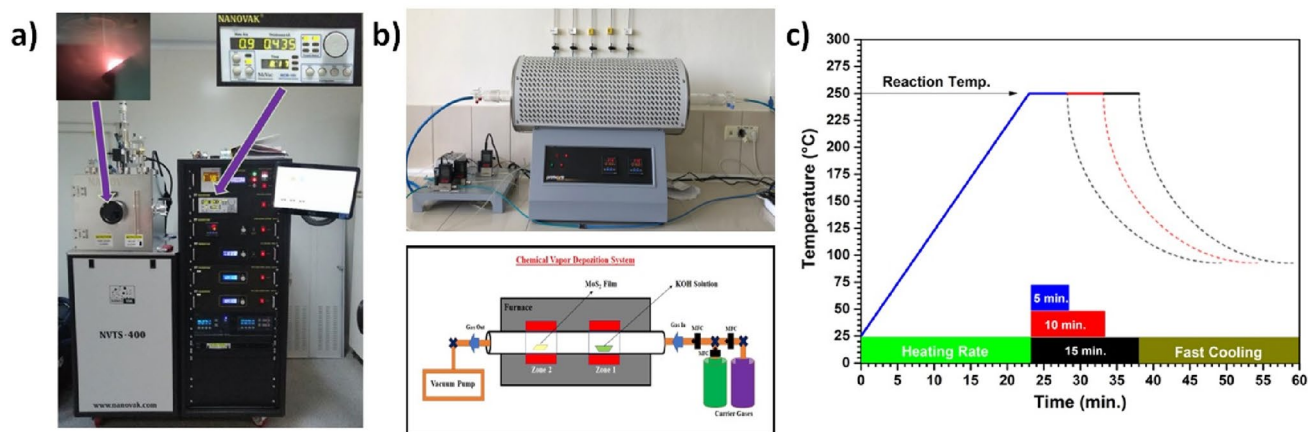

Fig. 1 PVD system (**a**), CVD system (**b**), and Annealing process of MoS_2 precursor films (**c**)

Table 3 The E_{2g}^1 and A_{1g} peak position of K-doped MoS_2 with molarity of 0.2-, 0.4-, 0.6-, and 0.8-M KOH for 5-min dwell time

KOH Ratio	Pristine	0.2 M	0.4 M	0.6 M	0.8 M
E_{2g}^1 (cm^{-1})	390	387	380	381	380
A_{1g} (cm^{-1})	410	409	404	405	404
Peak Diff.	20	25	24	24	24

Although, increasing molarity of the KOH was not affect the MoS_2 structure, the film homogeneity was affected seriously by variation of molarity. The peak positions of E_{2g}^1 and A_{1g} with respect to the molarity of KOH from varying from 0.2 M to 0.8 M, are given in Table 3. The Raman spectra of doped MoS_2 with 0.2–0.8 M KOH for 5 min at 250 °C revealed significant shifts in the E_{2g}^1 and A_{1g} peak positions. The E_{2g}^1 peak, corresponding to the in-plane vibration mode, shifted to approximately 380 cm^{-1} bands, while the A_{1g} peak shifted to the ~ 405 cm^{-1} bands, relative to the pristine MoS_2 E_{2g}^1 and A_{1g} modes. The shift of the E_{2g}^1 mode of K-doped MoS_2 compared to pristine MoS_2 indicates presence of Mo–K bond that generates a compressive effect [49]. Momose et al. [49] and Azcatl et al. [50] reported that induced strain by a single atom dopant in MoS_2 could be determined by Raman spectroscopy. They confirmed that the presence of foreign atoms can induce compressive strain in the MoS_2 structure. The A_{1g} peak position for 0.2-, 0.4-, 0.6-, and 0.8-M KOH-doped MoS_2 shifted about 6 cm^{-1}, which is also due to compressive strain effect and caused shift in the out-of-plane vibration mode A_{1g}. This situation might be partially attributed to the generate of K–Mo–K structure with K doping. In addition, A_{1g} was more sensitive to the doping. When the molarity of KOH was increased, the intensity of the A_{1g} peak in the Raman spectra also increased. Additionally, the A_{1g} peak was more significantly affected by the doping effects compared to other peaks. This observation suggests a strong interaction with electrons, indicating the influence of the doping process on the electronic structure of the MoS_2 [51, 52]. Therefore, A_{1g} Raman active signal intensity is lower than E_{2g}^1 Raman active signal because this peak is highly sensitive to doping effect. Additionally, another special peak observed at around 240 cm^{-1} for all K-doped MoS_2 films. This peak is attributed to the out-of-plane K–S Raman mode [32]. The MoS_2 species E_{2g}^1 and A_{1g} modes were disappeared for the 1-M KOH-doped MoS_2. This situation indicates the disruption of the S–Mo–S bond due to

increasing S–K bond and weakening S–Mo bond by K ion intercalations [53].

Raman spectrum analysis of pristine and potassium-doped MoS_2 films provided important insights into the effect of parameters on material performance. Shifts in the positions of E_{2g}^1 and A_{1g} peaks, associated with desorption and structural changes, show sensitivity to film layers and dopant concentration. The use of KOH solutions at different molarities affects the homogeneity of the films without significantly altering the MoS_2 structure. In particular, shifts in the Raman peaks indicate the presence of Mo–K bonds, inducing a compressive effect. The A_{1g} peak, which is particularly sensitive to doping effects, indicates a strong interaction with electrons, affecting the electronic structure of MoS_2. In addition, the appearance of a unique peak at 240 cm^{-1} indicates the out-of-plane K–S Raman mode.
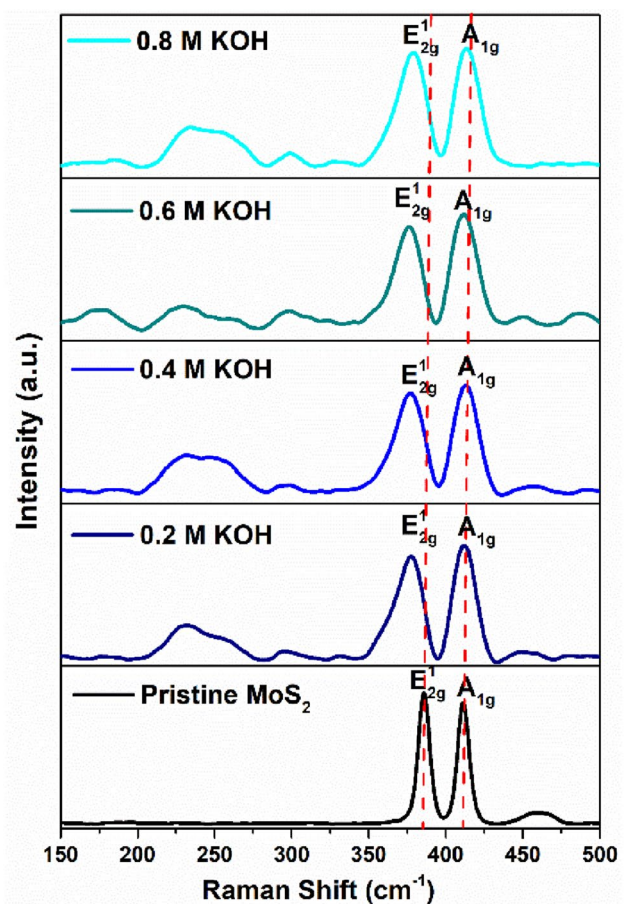
Fig. 2 Raman spectra of K-doped MoS_2 with 0.2-, 0.4-, 0.6-, and 0.8-M KOH for 5-min annealing dwell time

The Raman mapping revealed that the K-doped MoS_2 films were grown homogeneously on the substrate. Figure 3 displays the Raman maps of 0.2–0.8-M KOH-doped MoS_2 films obtained from the peak positions of E_{2g}^1 and A_{1g}. It was observed that the molarity of KOH significantly affected the homogeneity of the films. As the molarity of KOH increased, the film homogeneity decreased, and non-homogeneous areas of the films were indicated by dark black regions. Homogeneity loss can affect employability of MoS_2 in optoelectronic applications due to loss of electrical properties. Any loss of homogeneity in these aspects could potentially lead to variations in electrical and optical properties. For example, if there are regions within a MoS_2 material where the layer thickness deviates significantly from the desired uniformity, it might result in variations in electronic band structure, affecting the material's conductivity. Similarly, defects or impurities in non-uniform regions can introduce energy levels within the bandgap, influencing the material's optical properties. According to the Raman mapping of the films, K-doped MoS_2 films with 0.2-M KOH exhibited a higher degree of homogeneity and deteriorates with higher doping molarities. This could be attributed to toxic nature of KOH, thus damaging the MoS_2 structure at higher molarities [54]. In addition, more K atoms intercalating with increasing molarity of KOH may have destroyed the S–Mo–S structure. Given these conditions, the doping ratio of 0.2-M KOH was found to be the most suitable doping level for K-doped MoS_2 film.

The optical band gap of the MoS_2 film was determined by taking its optical transmission data. The absorption coefficient, α, was calculated using the Lambert–Beer law [55]. The optical band gap (E_g) of the MoS_2 films was obtained by plotting $(\alpha h\nu)^2$ against photon energy ($h\nu$) and considering the point of interception of the horizontal photon energy axis, as shown in Fig. 4. The optical band gap of the K-doped MoS_2 film was determined to be between 1.81 and 1.98 eV, which is consistent with previously reported experimental and theoretical studies [56, 57]. The doping and annealing treatment of MoS_2 have a significant impact on its band gap. The optical band gap of MoS_2 can be tuned by various parameters, such as annealing temperature, application of a magnetic field, excitonic coupling, doping, and electron or charge transfer [57]. In Fig. 4, it was observed that increasing the molarity of KOH caused a shift in the optical band gap from 1.98 to
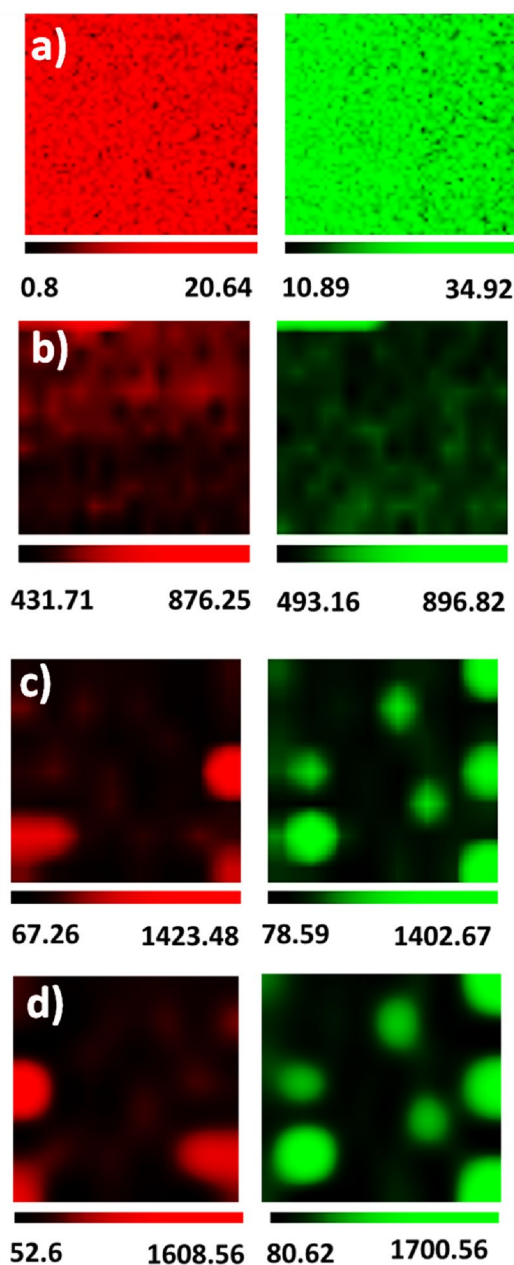

Fig. 3 Raman maps (50 × 50 μm) of K-doped MoS_2 films at different molarities for 5-min annealing dwell time. The red and green maps represent E_{2g}^1 and A_{1g} peak positions, respectively. **a** 0.2-M KOH, **b** 0.4-M KOH, **c** 0.6-M KOH, and **d** 0.8-M KOH (Color figure online)

1.81 eV. This shift in the optical band gap of K-doped MoS_2 may be related to the annealing temperature. When considering pristine MoS_2, temperature can cause the spectral absorption rate of excitons to decrease [58]. Additionally, the annealing temperature can affect the K point in the Brillouin zone of

Fig. 4 $(\alpha h\nu)^2$ versus photon energy ($h\nu$) plot for determination optical band gap of 0.2-, 0.4-, 0.6-, and 0.8-M KOH-doped MoS_2 for 5-min annealing dwell time
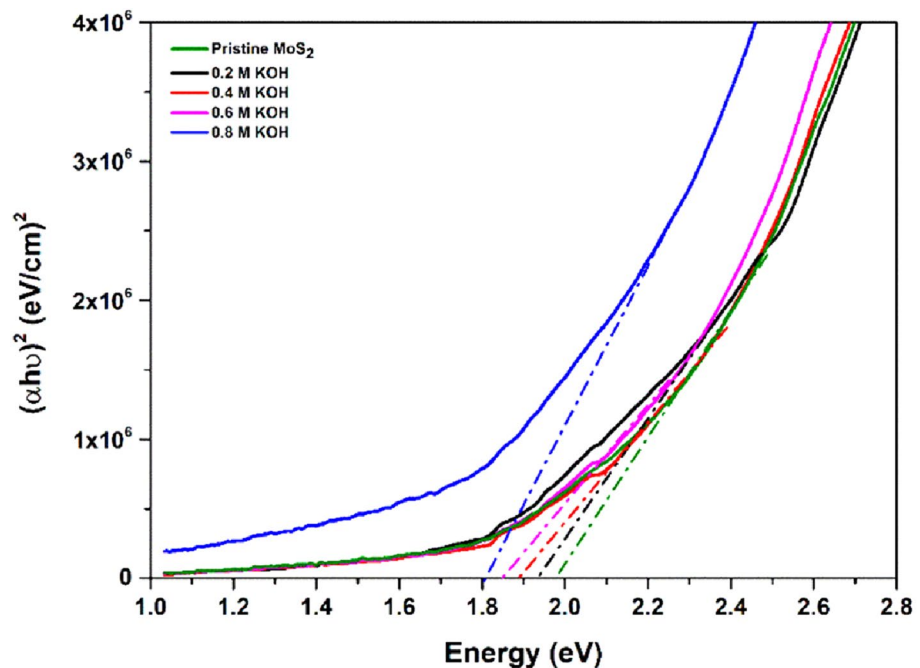
MoS_2. Conversely, red shifts are attributed to the Stokes shifts, and the magnitude of the Stokes shift is reported to increase with doping level [49, 59]. Therefore, the increase in KOH molarity may lead to more K atoms intercalating with MoS_2, resulting in a greater shift in the band gap, particularly for 0.8-M KOH-doped MoS_2. By doping the film with potassium, we are able to determine the band gap and find that the doping-induced energy shifts are strongly dependent on the orbital character of the bands. This situation provides interesting possibilities for tuning the band structure of MoS_2 and similar materials. This effect must be considered when placing MoS_2 between other materials [60].

Since the 0.2-M doped sample showed a more homogeneous distribution, the effect of annealing time was investigated using the sample with same amount doping. Raman spectra of MoS_2 films doped with 0.2-M KOH employing different annealing times (5, 10, and 15 min) as presented in Fig. 5. The E_{2g}^1 and A_{1g} peak positions and peak differences of K-doped MoS_2 with 0.2-M KOH annealed for 5-, 10-, and 15-min dwell times are given in Table 4. The peak positions of E_{2g}^1 and A_{1g} modes were determined at around 387 and 409 cm^{-1} for 5 min, and at around 391 and 413 cm^{-1} for 10 min of the annealing dwell times, respectively. There were no significant changes in the MoS_2 structure when the annealing

Table 4 The E_{2g}^1 and A_{1g} peak position of K-doped MoS_2 with 0.2-M KOH utilizing 5-, 10-, and 15-min annealing dwell times

Annealing dwell time (min.)	5	10	15
E_{2g}^1 (cm^{-1})	387	391	372
A_{1g} (cm^{-1})	409	413	409
Peak Diff.	22	22	27

dwell time was increased from 5 to 10 min. However, when the annealing time was further increased to 15 min, the MoS_2 structure was deteriorated, resulting in a significant decrease in the intensity of both Raman modes. The peak positions of E_{2g}^1 and A_{1g} modes determined as 372 and 409 cm^{-1}, respectively, for 5-min annealed sample. It was observed that the E_{2g}^1 and A_{1g} modes were seriously affected by increase in annealing time from 10 to 15 min, indicating an increased interaction between MoS_2 and K with longer annealing time. This suggests that the K atoms may penetrates the Mo atoms and significantly affected the MoS_2 structure. Moreover, the corrosive effect of the KOH may have caused to this phenomenon.

The Raman maps of the 0.2-M KOH-doped MoS_2 films which are annealed for 5-, 10-, and 15-min annealing times are given in Fig. 6. The Raman maps were obtained from the peak positions of the E_{2g}^1 and A_{1g}. The increasing of the annealing dwell time
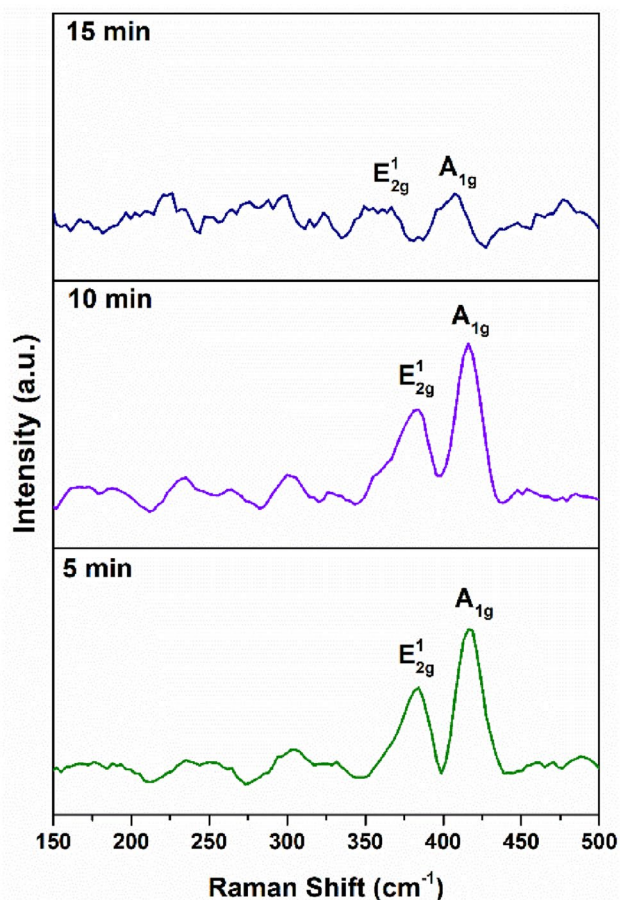
Fig. 5 Raman spectra of the K-doped MoS$_2$ with 0.2-M KOH employing 5-, 10-, and 15-min annealing times

Fig. 6 The Raman maps ($50 \times 50\,\mu$m) of 0.2-M KOH employing K-doped MoS$_2$ which are growth with different annealing dwell times: **a** 5 min, **b** 10 min, and **c** 15 min. The red and green maps represent E$_{2g}^1$ and A$_{1g}$ peak positions, respectively (Color figure online)

caused formation of inhomogeneous surface structure. The surface homogeneity of the MoS$_2$ films was turned into the non-uniform surface structure as the annealing time was increased. The dark regions indicated that the MoS$_2$ film structure was deteriorated, and 5-min annealing dwell time presented the most homogenous surface K-doped MoS$_2$ films according to the Raman mapping of the films. However, the longer annealing dwell time, the Raman intensity was started to decrease due to excessive damage of the film [39].

The optical band gap of the K-doped MoS$_2$ films grown with different annealing times were determined by optical transmission (T) data just like the doped MoS$_2$ films with different molarity of KOH. As shown in Fig. 7, the optical band gap of the K-doped MoS$_2$ determined between 1.71 and 1.9 eV. The optical band gap of K-doped MoS$_2$ films were affected with different annealing dwell times. When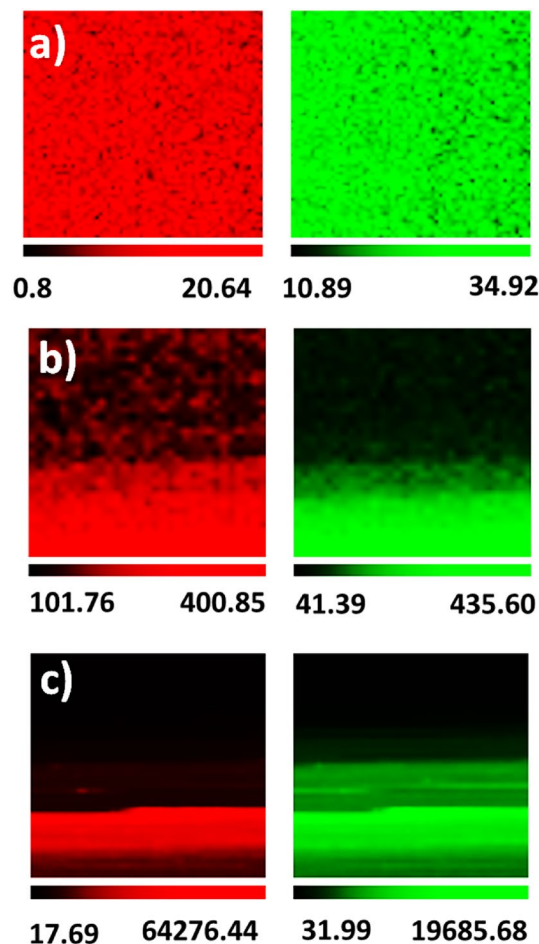 the annealing dwell times were increased, the optical band gap value of the films were shifted from 1.9 to 1.71 eV. Decreasing the band gap may be attributed to the spin-polarized density of states of the doped MoS$_2$ [61]. In addition, the K-doped MoS$_2$ film which is annealed with 15-min dwell time was exhibited lower optical band gap than others. This situation may be explained by decomposition of MoS$_2$ films. The MoS$_2$ show increase with the annealing time up to 15 min, due to formation of sulfur vacancies. So, the MoS$_2$ structure was affected, seriously. In this regard, the optical band gap of the films showed red shifting with increase in the annealing time. Considering all these conditions, the annealing time of 5 min was determined as the most appropriate annealing time for K-doped MoS$_2$ growth.

Fig. 7 $(\alpha h\nu)^2$ versus photon energy $(h\nu)$ plot for determination optical band gap of 0.2-M KOH employing K-doped MoS_2 with 5-, 10-, and 15-min annealing dwell times
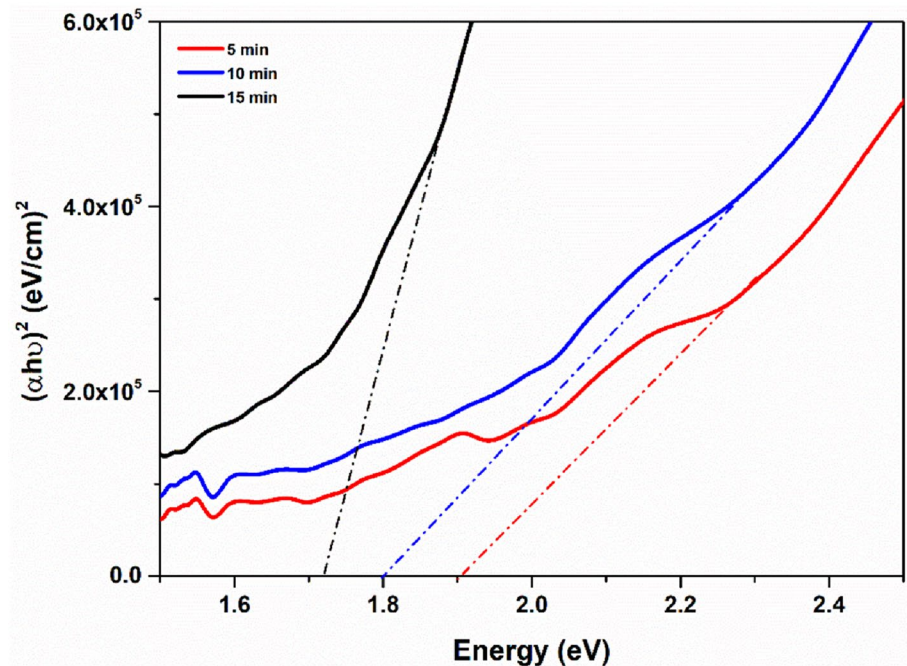
In summary, the optimal annealing time and KOH molarity for producing K-doped MoS_2 films are 5 min and 0.2 M, respectively. Longer annealing times and higher KOH molarity lead to deterioration of the MoS_2 structure, resulting in a decrease in the optical band gap and surface homogeneity. It is also important to use KOH with caution and to carefully monitor the annealing process to avoid damaging the MoS_2 films. The selection of doping concentration, annealing time, and other parameters significantly affects the performance of K-doped MoS_2. Striking a balance in these factors is essential for achieving the desired structural and electronic properties for specific applications, such as electronic or optoelectronic. These observations underscore the importance of fine-tuning parameters to enhance performance without compromising the material's integrity.

The XPS analysis performed for the K-doped MoS_2 film which was grown with the most promising molarity of KOH (0.2 M) and annealing time (5-min.) are shown in Fig. 8. The XPS spectrum (Fig. 8a) was showed that the surface of the material consists of only Mo, S, C, O, and K elements. The O and C elements occurred due to the glass substrate and reference C atoms. In Fig. 8a, the Mo 3d signal has three peaks, consisting of three separate overlapping and this situation showed Mo in three different oxidation states (Mo^{4+}, Mo^{5+} ve Mo^{6+}). The binding energies were

detected at 228.9, 230.1, and 223.6 eV that correspond to the structure Mo $3d_{5/2}$, Mo $3d_{3/2}$, and S 2s, respectively [62, 63]. The binding energies of the MoS_2 phase are generally between 228.9 eV and 232.1 eV and the binding energies of the MoO_2 phase are 229.3 and 232.4 eV [36]. Thus, these two phases are close to each other and difficult to distinguish. It was determined that the peaks obtained according to the XPS spectrum in Fig. 6b mainly correspond to the MoS_2 phase, not to the MoO_2 phase. In addition, K is a well-known electronic donor. When K is induced on the edge of MoS_2, it slightly donates a 4s valence electron into the empty d orbits of Mo. As a result, the electron density around Mo increases, leading to a slight decrease in the binding energy to 228.9 eV [64].

The peak shoulder of the S 2p XPS spectra is shown in Fig. 6c. Two different sulfur species were determined, in which the binding energy at 161.8 and 163.0 eV corresponds to the S $2p_{3/2}$ and S $2p_{1/2}$, respectively. In addition, these binding energies attributed to S^{2-} ion that can be found in K 2 S, MoS_2, and K–Mo sulfides [65–67]. From the XPS spectrum (Fig. 6d), K $2p_{3/2}$ peaks at 293.09 eV and K $2p_{1/2}$ peaks at 290.2 eV were detected. These results demonstrated that potassium has been effectively doped into the MoS_2, indicating the relationships of K with spin–orbit pairing [32]. When considering all these results permanent K-doped MoS_2 growth has been achieved.
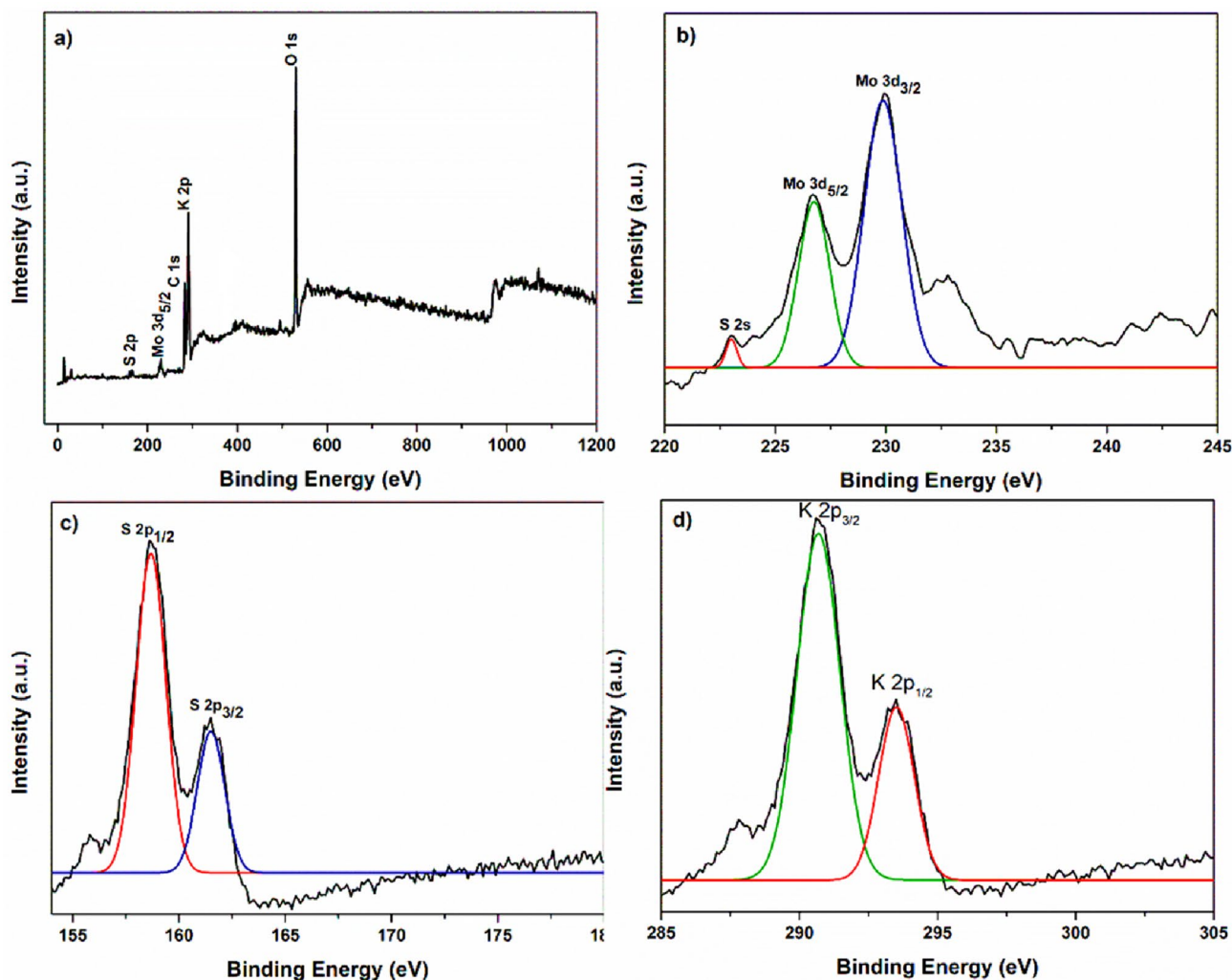
Fig. 8 a XPS spectrum of 0.2-M KOH employing K-doped MoS_2 for 5-min annealing dwell times **b** Mo 3d, **c** S 2p, and **d** K 2p XPS spectrum

4 Conclusion

The focus on K doping of MoS_2 films reveals its potential to enhance electronic and optical properties. Doping-induced energy shifts depend on the orbital character of the bands, offering opportunities for tuning the band structure. The study presents a two-step synthesis method for K-doped MoS_2 thin films, utilizing RF magnetron sputtering for deposition and CVD for K doping. By investigating the molarity of KOH and the dwell annealing time, consistent and permanent doping was achieved. The post-treatment method was used to achieve homogeneity and high-quality K-doped MoS_2 films. The molarity of KOH (0.2–0.8 M) and

annealing time (5–15 min) affected properties of the MoS_2 structure seriously. Increasing KOH molarity caused forming inhomogeneous surface structure of MoS_2 films. Therefore, 0.2-M KOH is used to grow K-doped MoS_2 film. The optical band gap observed that increasing the molarity of KOH caused a shift in the optical band gap from 1.98 to 1.81 eV. Besides, annealing time is essential parameter to grow K-doped MoS_2. The MoS_2 film structure deteriorated by longer annealing time. In this regard, 0.2-M KOH and 5-min annealing time were determined as the most promising parameters for growth K-doped MoS_2. The optical band gap value of the films was determined between 1.9 and 1.71 eV. After K doping, the optical band gap shifted approximately to

0.2 eV. Besides, permanent K-doped MoS$_2$ growth was confirmed by XPS measurement. K 2p$_{3/2}$ peaks at 293.09 eV and K 2p$_{1/2}$ peaks at 290.2 eV were detected in the XPS spectrum. These results demonstrated that potassium has been effectively doped into the MoS$_2$, indicating the relationships of K with spin-orbit pairing. Overall, homogeneous and permanent K-doped MoS$_2$ thin film was obtained by optimizing molarity of KOH and annealing time. In summary, the research underscores the significance of doping strategies in modifying the properties of MoS$_2$ films, particularly with K doping. The careful exploration of molarity and annealing time offers valuable insights into achieving optimal doping conditions for enhanced performance. The findings contribute to the broader field of 2D materials and nanotechnology, paving the way for technological advancements and innovative applications of K-doped MoS$_2$ films in various industries.

Author contributions

AA contributed to methodology, writing of the original draft, and writing, reviewing, & editing of the manuscript. SE contributed to data curation. MAO contributed to review & editing of the manuscript. GT contributed to data curation. RZ contributed to conceptualization and review & editing of the manuscript.

Funding

Data availability

The data that support the findings of this study are available on reasonable request from the corresponding author.

Declarations

Conflict of interest   The authors declare that they have no known competing financial interests or personal relationships that could have appeared to influence the work reported in this paper.

Ethical approval   This study does not contain any human-related information and no animals were used.

References

1. J. Wang et al., Transition metal dichalcogenides MX2 (M = Mo, W; X = S, Se, Te) and MX2-CIP composites: promising materials with high microwave absorption performance. J. Alloys Compd. **743**, 26–35 (2018)

2. T.A.J.E.T. Saleh, Nanomaterials: classification, properties, and environmental toxicities. Environ. Techno. Innov. **20**, 101067 (2020)

3. I. Gutiérrez-Lezama et al., Electroluminescence from indirect band gap semiconductor ReS2. 2D Mater. **3**(4), 045016 (2016)

4. H. Terrones, F. López-Urías, M.J.S. Terrones, Novel hetero-layered Materials with tunable direct band gaps by sandwiching different metal disulfides and diselenides. Sci. Rep. **3**(1), 1549 (2013)

5. K. Dolui, I. Rungger, S.J.P.B. Sanvito, Origin of the n-type and p-type conductivity of MoS 2 monolayers on a SiO 2 substrate. Phys. Rev. **87**(16), 165402 (2013)

6. S. Larentis, B. Fallahazad, E.J.A.P.L. Tutuc, Field-effect transistors and intrinsic mobility in ultra-thin MoSe2 layers. Appl. Phys. Lett. **101**(22), 223104 (2012)

7. T.A. Saleh, Protocols for synthesis of nanomaterials, polymers, and green materials as adsorbents for water treatment technologies. Environ. Technol. Innov. **24**, 101821 (2021)

8. A.A. Al-Qadri et al., CO_2 utilization in syngas conversion to dimethyl ether and aromatics: roles and challenges of zeolites-based catalysts. J. Energy Chem. (2023). https://doi.org/10.1016/j.jechem.2022.12.037

9. S. Wi et al., Enhancement of photovoltaic response in multilayer MoS_2 induced by plasma doping. Acs Nano **8**(5), 5270–5281 (2014)

10. S. Memaran et al., Pronounced photovoltaic response from multilayered transition-metal dichalcogenides PN-junctions. Nano Lett. **15**(11), 7532–7538 (2015)

11. K. Nassiri Nazif et al., High-specific-power flexible transition metal dichalcogenide solar cells. Nat. Commun. **12**(1), 7034 (2021)

12. D. Suthar et al., Correction: An overview on the role of ZnTe as an efficient interface in CdTe thin film solar cells: a review. Mater. Adv. (2022). https://doi.org/10.1039/D2MA00817C

13. J. Zhang et al., Enhanced second and third harmonic generations of vertical and planar spiral MoS_2 nanosheets. Nanotechnology **28**(29), 295301 (2017)

14. S.N. Shirodkar, U.V. Waghmare, Emergence of ferroelectricity at a metal-semiconductor transition in a 1 T monolayer of MoS 2. Phys. Rev. Lett. **112**(15), 157601 (2014)

15. X. Huang, Z. Zeng, H.J.C.S.R. Zhang, Metal dichalcogenide nanosheets: preparation, properties and applications. Chem. Soc. Rev. **42**(5), 1934–1946 (2013)

16. T.A.J.R. Saleh, Nanomaterials and hybrid nanocomposites for CO_2 capture and utilization: environmental and energy sustainability. RSC Adv. **12**(37), 23869–23888 (2022)

17. H. Wang, T. Maiyalagan, X.J.A. Wang, Review on recent progress in nitrogen-doped graphene: synthesis, characterization, and its potential applications. Acs Catal. **2**(5), 781–794 (2012)

18. M. Li et al., P-type doping in large-area monolayer MoS_2 by chemical vapor deposition. ACS Appl. Mater. Interfaces. **12**(5), 6276–6282 (2020)

19. S. Qin et al., In-situ and tunable nitrogen-doping of MoS_2 nanosheets. Sci. Rep. **4**(1), 1–5 (2014)

20. S. Jeon et al., Controlled p-doping of black phosphorus by integration of MoS_2 nanoparticles. Appl. Surf. Sci. **440**, 282–287 (2018)

21. Y.-C. Lin et al., Atomically thin heterostructures based on single-layer tungsten diselenide and graphene. Nano Lett. **14**(12), 6936–6941 (2014)

22. X. Ji et al., Post-synthesis Tellurium Doping Induced Mirror Twin Boundaries in monolayer molybdenum disulfide. Appl. Sci. **10**(14), 4758 (2020)

23. K. Dolui et al., Possible doping strategies for MoS_2 monolayers: an ab initio study. Phys. Rev. B **88**(7), 075420 (2013)

24. S.W. Han et al., Interface defect engineering of a large-scale CVD-grown MoS_2 monolayer via residual sodium at the SiO2/Si substrate. Adv. Mater. Interfaces **8**(14), 2100428 (2021)

25. Q.H. Wang et al., Electronics and optoelectronics of two-dimensional transition metal dichalcogenides. Nat. Nanotechnol. **7**(11), 699–712 (2012)

26. J. Xu et al., Interlayer nanoarchitectonics of two-dimensional transition-metal dichalcogenides nanosheets for energy storage and conversion applications. Adv. Energy Mater. **7**(23), 1700571 (2017)

27. B. Chamlagain et al., Mobility improvement and temperature dependence in MoSe2 field-effect transistors on parylene-C substrate. ACS Nano **8**(5), 5079–5088 (2014)

28. N. Saigal et al., Effect of lithium doping on the optical properties of monolayer MoS_2. Appl. Phys. Lett. **112**(12), 121902 (2018)

29. M.R. Laskar et al., p-type doping of MoS_2 thin films using Nb. Appl. Phys. Lett. **104**(9), 092104 (2014)

30. J. Chang et al., Atomistic simulation of the electronic states of adatoms in monolayer MoS_2. Appl. Phys. Lett. **104**(14), 141603 (2014)

31. R. Friend, A.J.A.P. Yoffe, Electronic properties intercalation complexes transition metal dichalcogenides. Adv. Phys. **36**(1), 1–94 (1987)

32. Z. Xu et al., The nature of K-induced 2H and 1T'-MoS_2 species and their phase transition behavior for the synthesis of methanethiol (CH3SH). Iscience **25**, 104999 (2022)

33. T. Miyake, S.J.P.R.B. Saito, Electronic structure potassium-doped carbon nanotubes. Phys. Rev. B **65**(16), 165419 (2002)

34. J. Kong et al., Alkaline metal-doped n-type semiconducting nanotubes as quantum dots. Appl. Phys. Lett. **77**(24), 3977–3979 (2000)

35. T. Yamada, Y. Okigawa, M.J.M.R.E. Hasegawa, Potassium-doped n-type stacked graphene layers. Mater. Res. Express **6**(5), 055009 (2019)

36. S. Erkan, A. Altuntepe, Z.A.N. Recep, Synthesis of MoS_2 thin films using the two-step approach. Niğde Ömer Halisdemir Üniversitesi Mühendislik Bilimleri Dergisi **12**(1), 297–301 (2023)

37. R. Kaindl et al., Growth, structure and stability of sputter-deposited MoS_2 thin films. Beilstein J. Nanotechnol. **8**(1), 1115–1126 (2017)

38. Z.J. Xiaoli, A review: the method for synthesis MoS 2 monolayer. Int. J. Nanomanuf. **10**(5–6), 489–499 (2014)

39. X. Wei et al., Mo–O bond doping and related-defect assisted enhancement of photoluminescence in monolayer MoS₂. AIP Adv. **4**(12), 123004 (2014)

40. B.R. Carvalho et al., Symmetry-dependent exciton-phonon coupling in 2D and bulk MoS₂ observed by resonance Raman scattering. Phys. Rev. Lett. **114**(13), 136403 (2015)

41. H. Li et al., From bulk to monolayer MoS₂: evolution of Raman scattering. Adv. Funct. Mater. **22**(7), 1385–1390 (2012)

42. K.-K. Liu et al., Growth of large-area and highly crystalline MoS₂ thin layers on insulating substrates. Nano Lett. **12**(3), 1538–1544 (2012)

43. I. Bilgin et al., Chemical vapor deposition synthesized atomically thin molybdenum disulfide with optoelectronic-grade crystalline quality. ACS nano. **9**(9), 8822–8832 (2015)

44. M.S. Kim et al., Photoluminescence wavelength variation of monolayer MoS₂ by oxygen plasma treatment. Thin Solid Films. **590**, 318–323 (2015)

45. C.-H. Lee et al., Atomically thin p–n junctions with Van Der Waals heterointerfaces. Nat. Nanotechnol. **9**(9), 676 (2014)

46. N. Choudhary et al., Growth of large-scale and thickness-modulated MoS₂ nanosheets. ACS Appl. Mater. Interfaces. **6**(23), 21215–21222 (2014)

47. W. Zhang et al., High-gain phototransistors based on a CVD MoS₂ monolayer. Adv. Mater. **25**(25), 3456–3461 (2013)

48. C. Lee et al., Anomalous lattice vibrations of single-and few-layer MoS₂. ACS nano. **4**(5), 2695–2700 (2010)

49. T. Momose et al., Phosphorous doped p-type MoS₂ polycrystalline thin films via direct sulfurization of Mo film. AIP Adv. **8**(2), 025009 (2018)

50. A. Azcatl et al., Covalent nitrogen doping and compressive strain in MoS₂ by remote N₂ plasma exposure. Nano Lett. **16**(9), 5437–5443 (2016)

51. B. Chakraborty et al., Symmetry-dependent phonon renormalization in monolayer MoS₂ transistor. Phys. Rev. **85**(16), 161403 (2012)

52. G. Kukucska, J. Koltai, Theoretical investigation of strain and doping on the Raman spectra of monolayer MoS₂. Phys. Status Solidi **254**(11), 1700184 (2017)

53. X. Wang et al., Atomic-scale clarification of structural transition of MoS₂ upon sodium intercalation. Acs Nano **8**(11), 11394–11400 (2014)

54. D. Peng, K. Liu, Solubility of monolayer MoS₂ and expected bioabsorbable LED. J. Phys.: Conf. Ser. **1739**, 012052 (2021)

55. P. Makuła, M. Pacia, How to correctly determine the band gap energy of modified semiconductor photocatalysts based on UV–Vis spectra. J. Phys. Chem. Lett. **9**, 6814–6817 (2018)

56. S.Y. Wang et al., Optical and electrical properties of MoS₂ and Fe-doped MoS₂. Jpn. J. Appl. Phys. **53**(4S), 04EH07 (2014)

57. F. Yan et al., Electron doping of semiconducting MoS₂ nanosheets by silver or gold nanoclusters. Langmuir **38**(14), 4378–4388 (2022)

58. G. Chen et al., Effects of deposition and annealing temperature on the structure and optical band gap of MoS₂ films. Materials **13**(23), 5515 (2020)

59. K.-I. Lin et al., Photoreflectance study of the near-band-edge transitions of chemical vapor deposition-grown mono- and few-layer MoS2 films. J. Appl. Phys. **119**(11), 115703 (2016)

60. J.A. Miwa et al., Electronic structure of epitaxial single-layer MoS₂. Phys. Rev. Lett. **114**(4), 046802 (2015)

61. Z. Wu et al., Resistive switching effect of N-doped MoS₂-PVP nanocomposites films for nonvolatile memory devices. AIP Adv. **7**(12), 125213 (2017)

62. T.A. Patterson et al., A surface study of cobalt–molybdena–alumina catalysts using x-ray photoelectron spectroscopy. J. Phys. Chem. **80**(15), 1700–1708 (1976)

63. D. Ganta, S. Sinha, R. T.J.S, 2-D material molybdenum disulfide analyzed by XPS. Surf. Sci. Spectra **21**(1), 19–27 (2014)

64. J. Lu et al., An exploration into potassium (K) containing MoS₂ active phases and its transformation process over MoS2 based materials for producing methanethiol. Catal. Today **339**, 93–104 (2020)

65. C. Liu et al., Potassium promotion effects in carbon nanotube supported molybdenum sulfide catalysts for carbon monoxide hydrogenation. Catal. Today **261**, 137–145 (2016)

66. C. Liu et al., Impact of potassium content on the structure of molybdenum nanophases in alumina supported catalysts and their performance in carbon monoxide hydrogenation. Appl. Catal. A Gen. **504**, 565–575 (2015)

67. J.E. Hensley, S. Pylypenko, D.A. Ruddy, Deactivation and stability of K-CoMoSx mixed alcohol synthesis catalysts. J. Catal. **309**, 199–208 (2014)